JOINT EUROPEAN TORUS

JET–P(90)28

J.A. Heikkinen, T. Hellsten, M.J. Alava
and JET Team

Fast Wave Absorption at the Alfven Resonance in ICRF Heating

Fast Wave Absorption at the Alfven Resonance in ICRF Heating

J.A. Heikkinen[1], T. Hellsten[2], M.J. Alava[3]
and JET Team*

JET-Joint Undertaking, Culham Science Centre, OX14 3DB, Abingdon, UK

[1]Technical Research Centre of Finland, Nuclear Engineering Laboratory,
P.O. Box 169, SF-00181 Helsinki, Finland.
[2]Royal Institute of Technology, Plasma Physics and Fusion Research, S-10044 Stockholm, Sweden.
[3]Helsinki University of Technology, Department of Technical Physics, Rakentajanauldo 2C,
SF-02150 Esopoo, Finland
** See Appendix 1*

Preprint of Paper to be submitted for publication in
Nuclear Fusion

ABSTRACT.

For ICRH scenarii having the majority cyclotron resonance intersecting the plasma core, mode conversion of the fast magnetosonic wave into an Alfven wave at the plasma boundary on the high field side takes place. Simple analytical estimates for the convened power in this mode conversion process are derived. In addition to the Budden parameter the convened power is found to depend only on the local absolute value of the fast wave electric field at the Alfven resonance. The effect of the reflection of the fast wave from the wall surrounding the plasma on the conversion is then easily explained. The results are compared with numerical calculations where fmite electron inenia and kinetic effects are included. The mode conversion is strongest for weak local density gradient, high density, and for resonances lying not too near the wall. Its dependence on parallel wavenumber turns out to be sensitive to the ion composition and on the exact location of the resonance. For first harmonic heating of tritium in a deuterium-tritium plasma in JET tokamak a nearly complete absorption of the power reaching the conversion layer is predicted for low parallel wavenumbers. This is a serious problem because of the weak absorption in the centre for this scenario.

1 Introduction

For some ICRH scenarii in small aspect ratio tokamaks the cyclotron frequency of the majority ions will at the high field side exceed the frequency of the launched wave. For such scenarii the magnetosonic wave intended to heat the centre of the plasma can undergo mode conversion into an Alfvén wave at the plasma boundary on the high field side. This gives rise to a parasitic damping of the magnetosonic wave. When the wave is not completely damped at its first pass across the centre of the plasma this parasitic damping press can become important even when the wave is launched from the low field side. Mode conversion at the high field side during ICRH occurs for scenarii for which the cyclotron resonance or its first harmonic lies close to the cyclotron resonance of the main plasma species. Examples of such heating scenarii in JET are: minority heating of D in T-plasmas, minority heating of ^{3}He in D-plasmas, minority heating of H in ^{3}He plasmas, first harmonic cyclotron resonance heating of T in D-plasmas. The mode converted Alfvén wave which propagates along the magnetic field lines can be absorbed by electron Landau damping and ion cyclotron damping or be mode converted into a slow electrostatic wave. In the case of mode conversion at the plasma boundary the slow wave propagates only in a thin limited space on the high field side of the mode conversion surface and will be absorbed or reflected at the plasma boundary. The reflected wave will in its turn undergo mode conversion to an Alfvén wave which is partly converted back to a magnetosonic wave. How serious this parasitic absorption mechanism is depends on how large a fraction of the total power is absorbed. This depends on the transmission of the magnetosonic wave through the centre of the plasma. For heating of ^{3}He minority at its fundamental cyclotron resonance in a D-plasma, the absorption or mode conversion at the centre is weak for waves with a low parallel mode number, but the transmission coefficient is small. For the larger parallel mode numbers the absorption is stronger. In this case the mode conversion at the plasma boundary becomes less important. For the first harmonic heating of T in a D-T plasma the absorption at the centre is weak and the transmission large, furthermore the mode conversion at the plasma boundary becomes comparable to the absorption in the centre. Hence, a large fraction of the total power can be absorbed there.

The mode conversion of the magnetosonic wave into an Alfvén wave for frequencies below

the cyclotron frequency of the majority species, for which a cut-off, resonance, cut-off triplet appears, was treated by Karney et al. [1] in a plane slab geometry. The 2-D mode conversion problem has been discussed in Refs. [2, 3, 4, 5]. In principle the fraction of the mode converted power could be calculated by using 2-D global wave codes treating the mode conversion as resonance absorption or by including a slow wave. However due to the large number of grid points required to resolve the Alfvén wave and the slow wave, it is not practical for realistic heating scenarii.

In the context of Alfvén wave heating the mode conversion at the Alfvén resonance is well studied in the literature [6] where this resonance is thought to give a major absorption mechanism of the wave. There, the angular frequency of the wave is well below the cyclotron frequency of the main ion species in which case the ensuing two cut-offs and the resonance of the fast wave form a closely spaced triplet. With density profiles allowing an asymptotic analysis of the incoming and outcoming waves the conversion, reflection and transmission fractions have been evaluated [1, 6]. In the present problem where the wave frequency is of the order of the ion cyclotron frequencies of the plasma, the width of the interaction region may be smaller than the wavelengths of the converted waves, and the proximity of the inner wall poses a reflective boundary condition for emanating waves, new problems arise. In Section 2 we present a simple analytical estimate for the conversion fraction in the present problem assuming a cold plasma and zero electron inertia. This estimate is tested against the numerical solution of the local wave equations where the assumption of zero electron inertia is relaxed and where the finite ion Larmor radius effects correct to second order in ion Larmor radius are included. In addition, a numerical survey of the most interesting aspects of this conversion is performed in Section 3. The relative absorption at the mode conversion and at the plasma centre are compared for relative ICRH scenarii.

2 Analytical estimates for the converted power

The propagation of magnetosonic waves in a plane geometry may adequately be described by the wave equation [7]

$$E_y'' + \frac{(S - n_z^2)^2 - D^2}{S - n_z^2} E_y = 0. \tag{1}$$

where E_y is the y-component of the magnetosonic wave in a coordinate system x, y, z denoting the radial, poloidal and toroidal directions, respectively. The prime denotes the derivation with respect to x and all the lengths are normalised to c/ω where c is the speed of light and ω is the angular frequency of the radiation. n_z is the refractive index of the wave along the background magnetic field assumed in z- direction. The poloidal refractive index n_y is assumed to be zero. S and D are defined as

$$S = 1 - \sum_i \frac{\omega_{pi}^2}{\omega^2 - \Omega_i^2}, \tag{2}$$

$$D = \sum_i \frac{\Omega_i}{\omega} \frac{\omega_{pi}^2}{\omega^2 - \Omega_i^2}, \tag{3}$$

where ω_{pi} and Ω_i are the plasma frequency and cyclotron frequency (of species i) respectively. The summation is taken over all species including the electrons. The fast wave branch is clearly propagating in density regions $S + D > n_z^2$ and $S - D < n_z^2 < S$ or $S - D > n_z^2$ and $S + D < n_z^2 < S$ depending on the relative signs of S and D. At $S = n_z^2$ which is the so called Alfve'n resonance (if $\omega < \Omega_i$ for majority ions) the dispersion relation has a singularity and it has been shown [6,8] that the power of the fast wave is taken away from it at this singularity. The inclusion of finite electron inertia and kinetic corrections in the corresponding wave equations allows the short wavelength modes to appear in the dispersion relation. The square of the refractive index in this limit near the Alfve'n resonance is sketched in Fig.1. By solving the wave equation, including the finite electron inertia or kinetic effects, it has been found that the wave power is converted at the $S = n_z^2$ resonance from a fast wave to short wavelength waves and the corresponding amount of power is transformed accordingly.

To assess the wave absorption at the singularity, we calculate the derivative of the real part of the Poynting flux $I' = Re(E_y^* B_z)'$, where $Re(\ )$ denotes the real part of the expression in the brackets, the * the complex conjugate, and B_z is the wave magnetic field component.

Using $B_z = -iE_y'$ we obtain $I' = Im(E_y^* E_y'')$ which can be written with the help of Eq.(1) as

$$I' = -Im[\frac{(S-n_z^2)^2 - D^2}{S-n_z^2}] \mid E_y \mid^2 . \tag{4}$$

The expression in the brackets is clearly real so that $I' = 0$ everywhere except at $S = n_z^2$. The change in the Poynting flux, i.e. the absorption fraction of the incoming wave, may therefore be calculated simply as an integral of I' over the singularity. Linearising $S = S_0 + S'x$, $D = D_0 + D'x$ around the point of the singularity $S_0 = n_z^2$ at $x = 0$ we obtain readily

$$\Delta I = \int_{-d}^{d} I' dx = \pi \frac{D_0^2}{S'} \mid E_y \mid^2, \tag{5}$$

which gives the absorbed (or converted) power as a function of local field and parameters at the singularity. We note that the expression in Eq.(5) shows the expected similarity with the result by Karney et al.[1] obtained for the conversion fraction C in a one-ion component plasma which can be written here in a general case as

$$C = \frac{\mid \Delta I \mid}{I} = 4.97 \frac{D_0^2}{\mid S' \mid} [\frac{\mid S' \mid}{S'^2 - D'^2}]^{1/3}. \tag{6}$$

This formula is obtained with the help of matched asymptotic expansions for the field by linearising the coefficient of E_y in Eq.(1) with respect to x and is limited to a case of an outgoing transmitted and converted waves.

For the applications of the present paper, the expression in Eq.(5) is more useful because of the possible reflection of the fast wave from the inner wall which is not included in the derivation of Eq.(6). The presence of the wall suppresses the wave field because of the boundary condition $E_y = 0$ at the wall. One can improve the estimate in Eq.(6) by requiring that the evanescent solution vanishes at the wall. In this way and following the derivation presented in Ref.[1] we obtain

$$C = \frac{\mid \Delta I \mid}{I} = 4.97 \frac{D_0^2}{\mid S' \mid} [\frac{\mid S' \mid}{S'^2 - D'^2}]^{1/3} \frac{[1 - \sqrt{3} Ai(L_w/h)/Bi(L_w/h)]^2}{1 + Ai(L_w/h)^2/Bi(L_w/h)^2}. \quad (7)$$

for the conversion fraction in the presence of reflection. Here L_w, which is normalised to c/ω, is the distance between the Alfve'n resonance and the wall. The incoming (+) and reflected (-) fast waves at the high density side are taken to be of the form $Ai(x/h) \pm iBi(x/h)$, where $Ai(z)$ and $Bi(z)$ are the solutions of the Airy equation $E_y'' - zE_y = 0$ (the coefficient of E_y in Eq.(1) is linearised) and $h = [\mid S' \mid /(S'^2 - D'^2)]^{1/3}$. On the low density side near the wall the evanescent waves are taken to be of the form $Ai(x/h)$ and $Bi(x/h)$. From Eq.(7) we see directly that $C \to 0$ as $L_w \to 0$, i.e. $E_y \to 0$ according to the estimate of Eq.(5), while C approaches the generalised Karney estimate in Eq.(6) as L_w increases. Note that the estimates in Eqs.(6) and (7) are valid at $D_0^2/ \mid S' \mid^{4/3} \ll 1$, i.e. at small C.

From the estimates in Eqs.(5)-(7) we see directly that the conversion becomes stronger at higher density and with weaker gradient of S according to the dependence on the Budden parameter $\eta = \pi D_0^2/ \mid S' \mid$. The dependence of C on n_z is more complicated. It was argued in Ref.[1] that the conversion increases for increasing n_z with plasmas of one ion component. However, in some many-ion component plasmas D_0 may locally increase for decreasing S_0, i.e. for decreasing n_z for the Alfve'n resonance at $S_0 = n_z^2$. In these cases D_0 is particularly sensitive to the magnetic field variation. For instance, in the case of first harmonic heating of T in DT-plasma η is maximised for small n_z while in the case of ^{3}He minority heating in D-plasma η is maximised for large n_z. These facts can be easily seen by inspecting the dependence of S_0 and D_0 on n_z with the constraint $S_0 = n_z^2$ for typical density and magnetic field profiles near the inner wall of a small aspect ratio tokamak for these heating schemes. It is clear that the conversion generally is stronger at resonances situating far inside the plasma due to larger density, weaker gradient of S and due to larger $\mid E_y \mid$, but can also become vanishingly small at $D_0 = 0$.

3 The Numerical Analysis

It was noted that the estimates in Eqs.(5)-(7) were derived in the cold plasma and zero electron inertia limit and Eqs.(6)-(7), particularly, for specific asymptotic behaviour in the

wave fields. It is of interest to study how good these estimates are if these conditions are relaxed. This leads us to the analysis of the full wave equations including finite temperature, finite electron inertia and arbitrary profiles for the background plasma parameters.

Neglecting magnetic shear and toroidicity one may write the wave equations including finite Larmor radius effects correct to second order in ion Larmor radius as [9]

$$-(\frac{d}{dx}+n_y)[\sigma(\frac{d}{dx}-n_y)](E_x+iE_y)$$
$$+(n_y^2+n_z^2-S)E_x+in_y\frac{dE_y}{dx}+iDE_y+in_z\frac{dE_z}{dx}=0 \tag{8}$$

$$i(\frac{d}{dx}+n_y)[\sigma(\frac{d}{dx}-n_y)](E_x+iE_y)$$
$$+in_y\frac{dE_x}{dx}-iDE_x-\frac{d^2E_y}{dx^2}+(n_z^2-S)E_y-n_yn_zE_z=0 \tag{9}$$

$$in_z\frac{dE_x}{dx}-n_yn_zE_y-\frac{d^2E_z}{dx^2}+(n_y^2-P)E_z=0, \tag{10}$$

where E_x, E_y and E_z denote the electric field components perpendicular to the magnetic field (x,y) and along it (z), respectively. n_z and n_y are the corresponding refractive indices of the radiation. A plasma slab inhomogeneous in the radial direction (x) is assumed. The dielectric tensor elements are given by

$$S=1+\sum_i\kappa_i[Z(a_{1i})+Z(a_{-1i})] \tag{11}$$

$$D=-\sum_i\kappa_i[Z(a_{1i})-Z(a_{-1i})]-\frac{\omega_{pe}^2}{\Omega_e\omega} \tag{12}$$

$$P=1-(\frac{\omega_{pe}^2}{\omega^2})a_{0e}^2Z'(a_{0e}) \tag{13}$$

$$\sigma=-\sum_i\kappa_ir_i^2[Z(a_{2i})+Z(a_{-2i})-Z(a_{1i})-Z(a_{-1i})], \tag{14}$$

where

$$\kappa_i=\frac{\omega_{pi}^2c}{2\omega^2n_zv_{Ti}}, \tag{15}$$

$$a_{ji} = \frac{1 - j\Omega_i/\omega}{n_z v_{Ti}/c}, \tag{16}$$

$$a_{0e} = c/n_z v_{Te}, \tag{17}$$

and Z denotes the complex-valued plasma dispersion function and summation extends over all ion species. v_{Ti}, ω_{pi} and Ω_i are the thermal velocity, plasma frequency and cyclotron frequency of the i'th species (i=e, for electrons), c is the speed of the light. All the lengths are normalised to c/ω. r_i denotes the ion Larmor radius $(v_{Ti}/\sqrt{2}c)(\omega/\Omega_i)$.

For typical plasma density and temperature profiles in tokamaks the edge gradients are usually excessively large to make even the WKB approximation acceptable for describing the wave behaviour. To assess the converted power or absorbed power at the Alfve'n resonance, the full wave equations of Eqs. (8)-(10) should be solved over the conversion region. The problem which arises concerns the boundary conditions with which Eqs. (8)-(10) should be solved. To avoid solving these equations over the whole plasma one should have reliable analytical estimates for the wave behaviour far from the resonance but sufficiently near it (to make the integration length short and the physics simple enough). We propose here boundary conditions in which the wave decomposition to the three wave branches is made at the both ends of the calculation region. The short wavelength branches can be described by the WKB approximation; $E'_{xs} = in_{xs}E_{xs}$, $E'_{xB} = in_{xB}E_{xB}$, where E_{xs}, E_{xB} and n_{xs}, n_{xB} refer to the x- component of the electric field and the refractive index, respectively, of the slow (s) and ion Bernstein (B) wave branches, and the prime denotes derivation with respect to x. The corresponding fast wave branch can be described by the Airy function solutions $Ai(z) \pm iBi(z)$ for the right going (+) and left going (-) waves. Here $Ai(z)$ and $Bi(z)$ are the solutions to the Airy equation $E''_{yf} - zE_{yf} = 0$ with $z = -n^2_{xf}/C^{2/3}$. n^2_{xf} is equal to the coefficient of E_y in Eq.(1), and $C = -d(n^2_{xf})/dx$. If $n^2_{xf} < 0$ is valid, one should use $Ai(z)$ for the right evanescent wave and $Bi(z)$ for the left evanescent wave. Alternatively, to test the effect of the boundary conditions we have determined E'_{yf}/iE_{yf} directly by taking it equal to n_{xf} which applies if weak gradients at the boundaries are preferred. In the following the latter boundary conditions are called as homogeneous while those relying on the use of the Airy function solutions are called as Airy conditions. The polarisations of the wave branches are easily assessed from Eqs.(8)-(10) with the assumed wave forms.

We note that the kinetic effects are introduced via the terms proportional to σ while the finite electron inertia effects are equivalent to including E_z in the equations i.e. having finite P. Eqs.(8)-(10) reduce to Eq.(1) in the limit $\mid P \mid \rightarrow \infty$ and $\sigma \rightarrow 0$ as can be seen by putting $E_z = 0$, $\sigma = 0$ and by solving Eq.(8) for E_x and substituting it into Eq.(9).

By solving Eqs.(8)-(10) with the finite element method [9,10] and by using the above boundary conditions we are able to calculate the conversion, reflection and transmission for a given incoming fast wave power flux with sufficient accuracy and with reasonable computing time for routine runs. The boundaries of the computation region have to be set on such regions near the conversion layer that they are valid with sufficient accuracy. This requires that no cut-offs nor resonances nor wave transformation points do lie near the boundary. The zeros of S and σ are also avoided. The calculations include the possibility of an incoming fast wave at both boundaries to allow the reflection from the walls or cut-offs outside the calculation region. This is easily accomplished by decomposing the wave at the boundaries to left- and right-going waves in addition to the branch decomposition. For the short wavelength waves this is hardly necessary due to their local absorption and due to the fact that their group velocity predominantly lies along the magnetic field lines.

The calculation can be done in a plane approximation which, however, may not accurately describe the absorption of the short wavelength waves. Their propagation is strongly affected by the toroidicity, and a 2-dimensional calculation would be needed [2,3]. However, we believe that the 1-dimensional calculation is sufficient for estimating the conversion fractions of the incoming power, and a separate analytical study could be done to estimate the absorption of the short wavelength modes.

To solve Eqs.(8)-(10) across the Alfve'n resonance we have chosen suitable profiles for the density and temperature near the inner wall using the data of JET. At the low density boundary we have chosen the inner wall where a complete reflection for the magnetosonic wave is assumed while the short wavelength waves are assumed to escape freely the interaction region. Fig.3 shows graphs of the electric field components as calculated from Eqs.(8)-(10) in the case of ^{3}He minority heating in a D plasma for 5% ^{3}He concentration. The chosen density profile $N(x)$ is depicted in Fig.2. N is assumed to decrease exponentially from $1.6 \times 10^{19}\mathrm{m}^{-3}$ to $5.3 \times 10^{17}\mathrm{m}^{-3}$ in a region from $x = 0$ to $L = 0.04$cm and is assumed to have a constant value from $x = 0.04$cm up to the inner wall at $L+a = 0.06$cm.

$\omega = 2.1 \times 10^8 s^{-1}$ and $B = 5.5$T for the local magnetic field are assumed. The temperature $T = 50eV$ is taken and homogeneous boundary conditions are used. The locations of the Alfve'n resonance and the cut-offs are shown with the chosen $n_x = 8$ and $n_y = 0$. The graphs of E_x and E_z which characterise the slow wave branch, show clear mode conversion around $S = n_z^2$. E_y, which is mainly due to the fast wave component, is suppressed by the proximity of the metal boundary and decays smoothly over the calculation region, due to the long wavelength of the fast wave. No remarkable change in the results was found as the integration was started from higher or lower density with the same density profile as long as it includes the $S = n_z^2$ resonance.

In Fig.4 the fraction C of the incoming power that is converted to the slow wave branch is shown for the case of Fig.3 as a function of the length L of an exponentially decreasing density region and of the length a of the constant density region. The dependence on a is clearly due to dependence of the amplitude of E_y in the mode conversion layer on the proximity of the metal boundary. When a becomes several fast wave (evanescent) wavelengths C becomes more and more insensitive to a, as expected. With small a the conversion strongly decreases with a because of the decrease of $\mid E_y \mid$ according to the estimate in Eq.(5). For comparison we have shown in Fig.4 the prediction for C as calculated from Eq.(7). This estimate is found to describe well the functional dependence of C on a. The values from the numerical solution are larger by a factor of two, approximatively, which was found to be due to the boundary conditions and the linearisation of S and D applied in the derivation of Eq.(7). On the other hand it was found that the numerical results agree with the estimate in Eq.(5). Extending the exponential density region by increasing L (with the same density profile) increases the conversion at small a because the distance between the metal boundary and the mode conversion layer increases. At large a where this distance is not important one observes a slight reduction in conversion as L increases.

The effect of density gradient on the conversion at the Alfve'n resonance is clearly pictured in Fig.5 where we have modelled the density profile as $N(x) = 1.6 \times 10^{19} exp(-gx/L) \mathrm{m}^{-3}$ and show the conversion fraction as a function of L for $g = 3.4$ and 4.6. The other parameters are the same as in Fig.3. The conversion increases as a function of L more or less linearly in the depicted region according to the estimate of Eq.(5). For better comparison, the corresponding curve for large a is shown for $g = 3.4$. This curve is free

from the wall effects and makes the quantitative comparison possible to both estimates in Eqs.(5) and (6). With the help of Eq.(5) one may write the converted fraction C of incoming power as $-\Delta I/I$, where I is the total Poynting flux coming towards the resonance and ΔI is the change in the flux across the resonance. This is given by

$$C = \pi \frac{D^2}{\mid S' \mid n_{xf}} \frac{\mid E_y \mid^2}{\mid E_{y0} \mid^2}, \tag{18}$$

where D, $S' = dS/dx$ and E_y are calculated at the resonance $S = n_z^2$ while n_{xf} and E_{y0}, the perpendicular refractive index and the y-component of the electric field of the fast wave, are calculated at the boundary through which the incoming power is coming. This is an accurate expression for the conversion in the limits of cold plasma and $\mid P \mid \rightarrow \infty$, where the electron inertia and, correspondingly, E_z can be neglected. C from this formula is shown in Fig.5 (for large a) and shows a similar trend as C from the numerical calculations. However, the obtained values from this estimate are somewhat larger than from the numerical calculations. By taking the limit $\mid P \mid \rightarrow \infty$ in the numerical calculations we found a good quantitative agreement between the numerical values and the estimate in Eq.(18) showing that the observed discrepancy in Fig.5 (and also in Fig.4) is due to finite electron inertia. The obtained P dependence of C for $n_z = 8$ and $L = 4$cm is sketched in Fig.6 and has an asymptotic value for C which equals the value predicted by Eq.(18) in Fig.5. Finite electron inertia effects were discovered to be particularly important at small n_z and at steep gradients where the estimate in Eq.(18) still gave the correct scaling but its magnitude could deviate even by a factor of two from the correct result. In the limit $P \rightarrow \infty$ the results again agreed poorly with the estimate in Eq.(6), because of the different boundary conditions. In fact, by using the Airy boundary conditions in the numerical calculations a much better agreement was found in this limit. For typical values $L = 4 - 8$cm and $a = 2 - 10$cm, a conversion fraction of $5 - 10\%$ is obtained from Figs. 4 and 5 for $n_z = 8$.

The dependence on n_z is shown in Fig.7 for the parameters of Fig.3. C generally increases as n_z increases. This reflects the density dependence of C which is nearly linear according to Eq.(5) for an exponential density profile. Note that the Alfve'n resonance $S = n_z^2$ is situated at higher densities at larger n_z. At small n_z less than about 4 the conversion is zero because the slow wave becomes evanescent at the constant density regime and there

is no Alfve'n resonance in the chosen density region. This feature is partly unphysical because the density obviously continues to decrease down to the metal boundary. However by extending the exponential decrease of the density nearer to the wall, a similar decrease of C with n_z was found as shown in Fig.7. The small hump in C at $n_z = 5$ was found to be caused by the change from the evanescent fast wave to a propagating one at the low density region. At sufficiently high n_z the fast wave becomes evanescent at the high density boundary at $x = 0$ as calculated from Eq.(1). Therefore the curve has not been extended over $n_z = 10$. However, in real circumstances the density still increases towards the plasma centre and n_{xf} certainly has a non-zero real part also for somewhat higher n_z. Some results for higher n_z up to $n_z = 12$ are shown when n_{xf} was arbitrarily fixed to $n_{xf} = 10$ and 2. These results show that C still increases as a function of n_z. The corresponding curve for C at large a is also depicted together with the predictions from the estimate in Eq.(18). A similar agreement as in the previous figure was obtained between the estimates of Eqs.(18), (6) and the numerical results with large a.

We note that in all the previous calculations the reflectivity $\mid R \mid^2$ is found to be equal to $1 - C$, as expected because no net power is actually allowed to be transmitted across the conversion layer. The only exceptions are those cases where the slow wave is allowed to be reflected from the boundary in which case $\mid R \mid = 1$ is obtained and the case where both waves are allowed to escape from the boundary. If the escaping fast wave in this case is propagating the energy conservation $1 = \mid R \mid^2 + \mid T \mid^2 + C$ is accurately found with T denoting the transmitted field.

As a second example, a D-T plasma with the first harmonic heating of tritium in JET configuration is analysed. In this case with equal amounts of deuterium and tritium, S is negative near the boundary but can be positive near the deuterium cyclotron resonance layer which in typical JET configuration in this heating scheme would lie at about 40cm inwards from the inner wall. Mode conversion layer in this case is modelled with a locally linearly decreasing density profile $10^{19}[1-x(\mathrm{m})/0.2]\mathrm{m}^{-3}$ and with a model $5.15 \times R/(R-x)$ Tesla for the spatial dependence of toroidal field with R denoting here the major radius at $x = 0$. $R = 2\mathrm{m}$ is chosen with a temperature of 500eV and with $\omega = 2.1 \times 10^8 \mathrm{s}^{-1}$ for calculations. The calculation is performed in the region from $x = 0$ to $x = L = 0.1\mathrm{m}$ and the wall is taken to be at $x = L + a$ with $a = 0.1\mathrm{m}$. Fig.8 shows the conversion fraction as a function of n_z for the case of reflection and without it. The results are shown

for homogeneous and Airy boundary conditions. They do not differ much for these two boundary conditions making the present calculation method reliable for the evaluation of the conversion over a limited plasma layer at the tokamak edge. We note that C shown in Fig.8 is computed by reducing the power fluxes carried by the fast waves going out of the plasma layer from the incoming fast wave power fluxes and dividing this difference by the incoming (excluding the reflected wave from the wall) fast wave power flux. C therefore also includes the possible damped fraction of the wave power fluxes. For larger n_z (> 6) electron Landau damping of the electrostatic waves can play a role in the present case. By defining P as purely real in our computations we found the same C as shown in Fig.8 but now this fraction corresponded exactly to the fraction of the outgoing electrostatic wave power fluxes as expected. In the case of complex P the converted waves were nearly completely absorbed for $n_z \geq 8$ within the computation region.

The effect of reflection of the fast wave from the wall differs clearly from the case of ^{3}HeD-plasma where the resonance lies near the wall. In the present case the resonance lies sufficiently far away from the wall so that the local value of $\mid E_y \mid$ actually oscillates as a function of the optical length from the resonance to the wall. This is demonstrated in Fig.9 where the same density profile as in Fig.8 extending up to $L = 10$cm and continuing as constant from $L = 10$cm to $L = 10$cm$+a$ was used for the same case with $n_z = 2$. The converted power clearly oscillates as a function of a because n_f at the constant density region in this case is real making $\mid E_y \mid$ to oscillate between zero and some maximum value at the resonance. The obtained values of C agreed with those of the estimate in Eq.(18) with good accuracy thus proving the $\mid E_y \mid$ dependence. The conversion without the reflection shown in Fig.8b has a small trend to increase as a function of n_z. The Budden parameter actually is larger for smaller n_z in this case but the length of the evanescent region in front of the resonance between the fast wave cut-off and the resonance rapidly increases for increasing n_z making $\mid E_y \mid$ to decrease at the resonance. Due to these counteracting effects we obtain the slight increase in C for increasing n_z in Fig.8b. A good agreement with the estimate in Eq.(18) was again found proving the reasoning. The increase in C at low n_z in Fig.8a with reflection is explained by the obtained maximum for C for the chosen $a = 10$cm and $n_z = 2$ as shown in Fig.9. For $n_z = 8$ the corresponding maximum is somewhat shifted and a smaller increase in C is obtained with reflection. The small differences in Fig.8 for the two different boundary conditions can also be explained with this reasoning. The results in this case were not sensitive to the value of P explaining

the good agreement with the estimate in Eq.(18). Note that the converted wave in this case turns out to be an ion Bernstein wave due to the proximity of $S = 0$ layer to the Alfve'n resonance. As is known the slow wave can be transformed (and transmitted) to a kinetic wave through the $S = 0$ layer or be reflected as a kinetic wave depending on the sign of σ. This can be important from the point of view of damping of the short wavelength waves.

The case of first harmonic heating of ^{3}He in H-plasma is shown in Fig.10. Here the results show strong conversion as in the case of first harmonic heating of T in D-plasma as is expected because the cyclotron frequencies are doubled for both ion species. In fact, a correspondence between these two cases should be obtained by having a two times larger H density than D density and the same ^{3}He density as T density in these schemes in which case the dielectric tensor elements S and D are the same for these schemes. However the dependence of C on n_z in the case of reflection is now somewhat opposite to that in the case of DT- plasma which is due to the change in the optical length for the reflected wave. Again a good agreement with the estimate in Eq.(18) is found. The large values of C for $n_z = 8$ and 10 in the case of no reflection are caused by our choice $L = 15$cm in the calculations. For $n_z \geq 8$ the fast wave becomes evanescent at the low density boundary and a natural reflection results simulating the wall effect. In the present case σ happens to have a zero near the zero of S in the vicinity of the Alfve'n resonance. At small n_z the converted wave emanates out from the right boundary in the form of ion Bernstein wave polarization while for $n_z > 2$ it propagates out from the left boundary in the same polarization.

4 Conclusions

According to the shown results the Alfve'n resonance on the high field side of a small aspect ratio tokamak may cause strong local absorption of the heating wave in ICRH for some specific heating scenarios. In the case of first harmonic heating of tritium in DT-plasma the cyclotron absorption varies between 5% and 40% for typical JET parameters while the TTMP/electron Landau damping varies between 7% and 20%. Due to the large transmission much power may reach the Alfve'n resonance where a nearly complete

absorption for low n_z in JET configuration is predicted according to our results. An equally strong conversion is obtained for first harmonic heating of ^{3}He in H-plasma which could serve as a test case in the present inactive phase of experiments. For the heating scenarios having the resonance very near the wall like in D minority heating in DT-plasma or ^{3}He minority heating in D plasma our results predict a fairly small conversion at the Alfve'n resonance. This is due to the lower local density, steeper gradients and due to the presence of the reflecting inner wall of the tokamak.

A good agreement between our numerical results and analytical estimates including the wall effect are found. In particular, the agreement is found with an estimate for the converted power which predicts a linear dependence on the Budden parameter and on $\mid E_y \mid^2$ as calculated at the resonance. The latter dependence fully explains the wall effect on the conversion. For resonances lying very near the wall the conversion is suppressed by the small value of $\mid E_y \mid$ while for resonances far away from the wall the local field value is determined from the standing wave pattern formed by the wall, antenna and the cut-offs of the fast wave. Our results indicate a fairly complicated dependence of the conversion on electron inertia. By multiplying the true P by an arbitrary real number C was found to oscillate as a function of this number and to approach our analytical estimates derived in the limit of zero electron inertia by making $\mid P \mid$ very large. However in the studied cases this oscillation did not cause large deviations from the analytical predictions. Therefore, we expect that the formula in Eq.(5) could be used to simulate the conversion at the Alfve'n resonance in the complex 2-dimensional codes solving the waves in ICRH of tokamaks with a modest grid size. Anyway a more careful inspection of kinetic and finite electron inertia effects is needed to improve the analytical estimates.

ACKNOWLEDGEMENTS

This work was done under the JET Contract No. JT9/14673 at the Technical Research Centre of Finland and Helsinki University of Technology. The authors wish to thank Dr. D.F. Düchs and Dr. L-G. Erikson for their constant support and encouragement during this work.

J.A. Heikkinen and M.J. Alava are also grateful to Prof. R.R.E. Salomaa and Dr. S.J. Karttunen for their interest and support in the course of this work.

REFERENCES

[1] KARNEY, C.F.F., PERKINS, F.W. and SUN, Y.C., Phys.Rev.Lett. **42** (1979)1621.

[2] HELLSTEN, T. and TENNFORS, E., Physica Scripta **30** (1984) 341.

[3] HELLSTEN, T. and VILLARD, L., Nuclear Fusion **28** (1988) 285.

[4] TENNFORS, E., Plasma Phys. Contr. Fusion **28** (1986) 1483.

[5] APPERT, K., HELLSTEN, T., VACLAVIK, J. and VILLARD, L., Plasma Phys. Contr. Fusion **30** (1988) 1195.

[6] STIX, T.H. and SWANSON, D.G. in "Handbook of Plasma Physics", Vol.I, 1983, Ch.2.4.

[7] STIX, T., "The Theory of plasma waves", McGraw-Hill Book, New York, 1962.

[8] BUDDEN, K.G., "Physics of the Ionosphere", Physical Society, London, 1955, p.320.

[9] BRAMBILLA, M., Nuclear Fusion **28** (1988)549.

[10] APPERT, K., HELLSTEN, T., VACLAVIK, J. and VILLARD, L., Comp. Phys. Comm. **40** (1986) 73.

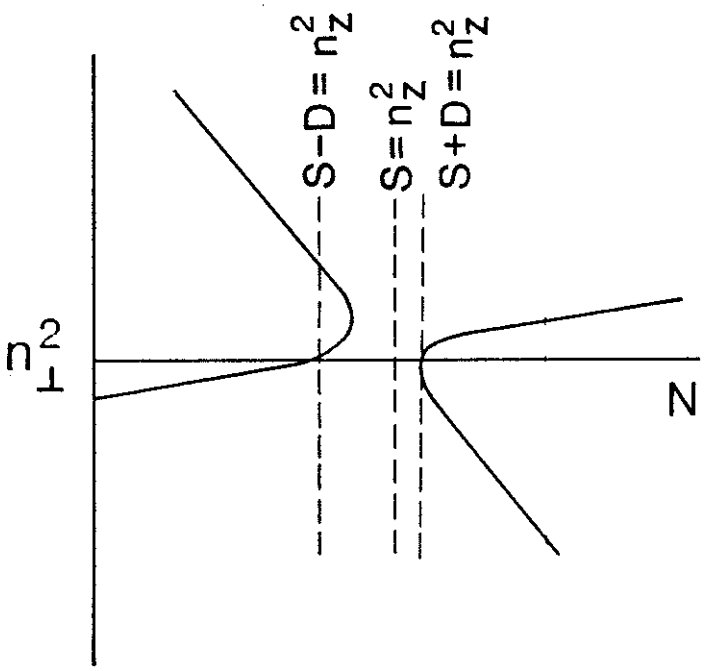

Fig.1 The square of the refractive index near an Alfve'n resonance as a function of density N(x). The fast wave and slow wave branch are shown.

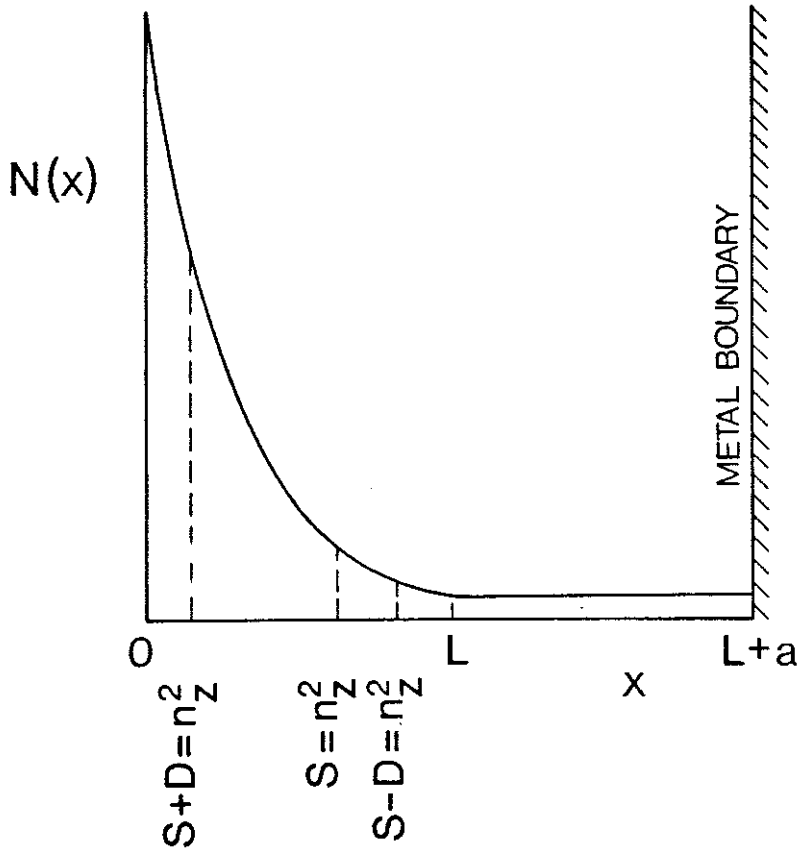

Fig.2 The mode conversion geometry with a model density profile for calculations.

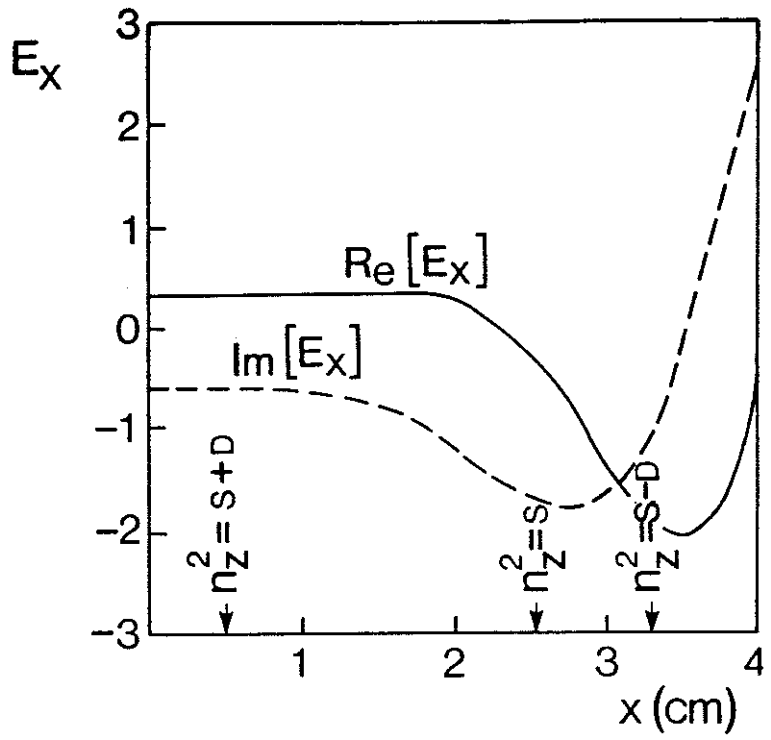

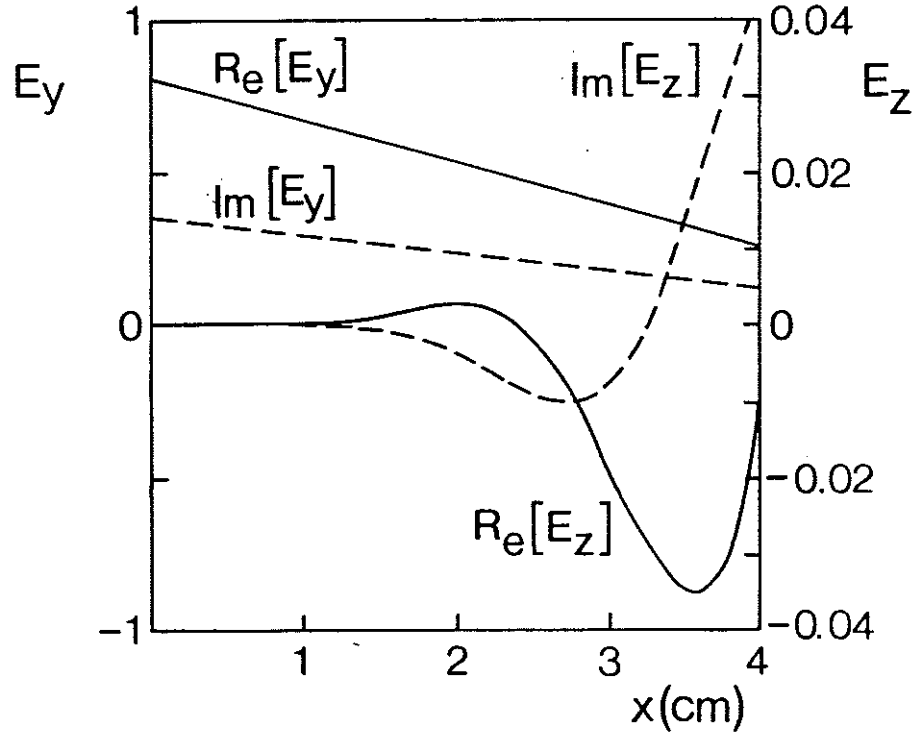

Fig.3 The graphs of the real and imaginary parts of E_x, E_y and E_z as computed from Eqs.(8)-(10) for D(^{3}He) plasma with 5% ^{3}He concentration. The density decreases exponentially from $1.6 \times 10^{19}\mathrm{m}^{-3}$ at $x = 0$ to $5.6 \times 10^{17}\mathrm{m}^{-3}$ at $x = 4$cm, and remains constant from $x = 4$cm to $x = 6$cm. The other parameters are $\omega = 2.1 \times 10^8\mathrm{s}^{-1}$, $B = 5.5$T, $n_z = 8$, $n_y = 0$.

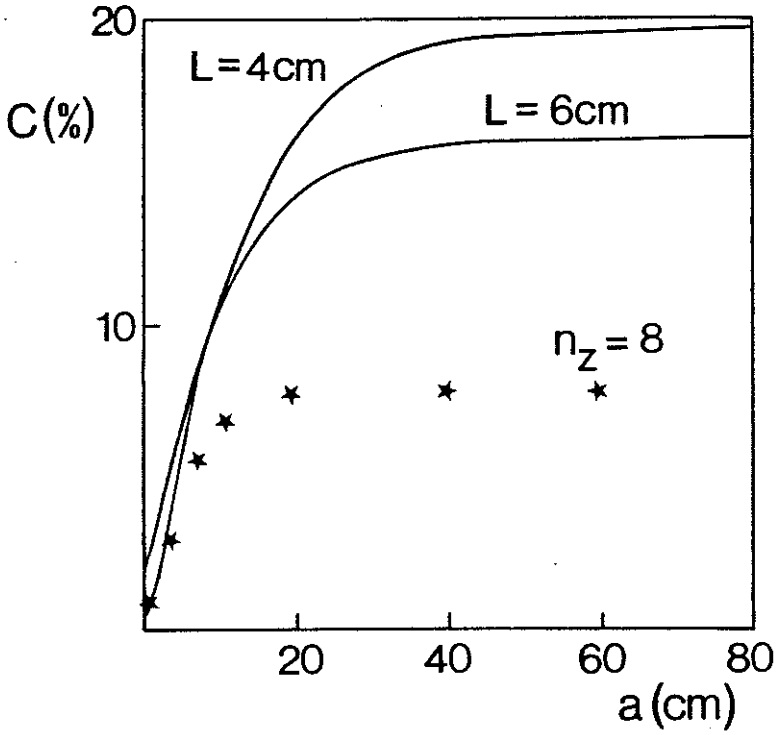

Fig.4 The conversion fraction C as a function of a for $L = 4$cm and for $L = 6$cm. The other parameters are the same as in Fig.3. The prediction of the estimate in Eq.(7) is shown for $L = 4$cm ($\star$).

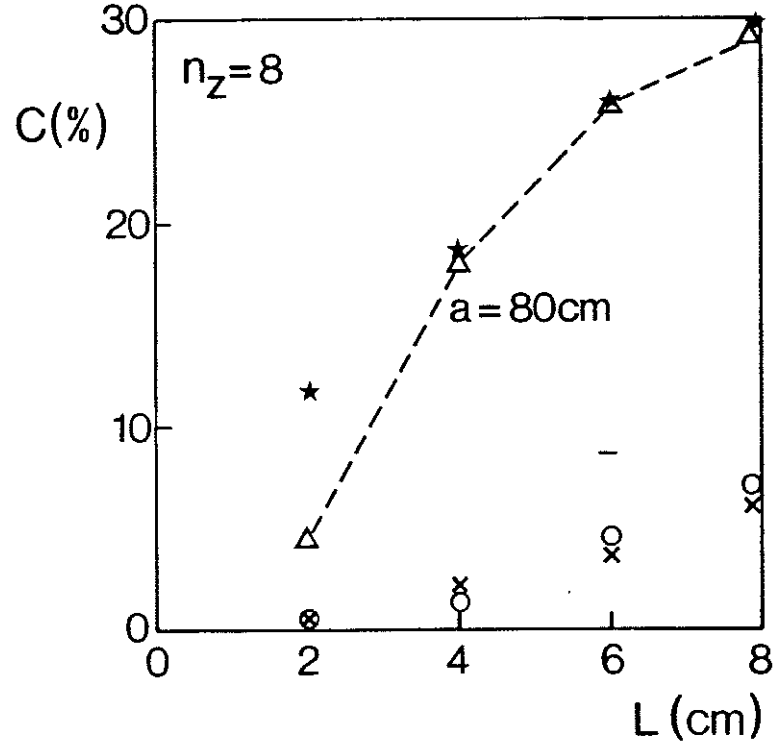

Fig.5 The effect of density gradient on C for model density profile $N(x) = 1.6\times10^{19} exp(-gx/L)\mathrm{m}^{-3}$ with $g = 3.4$ (x) and 4.6 (o). The other parameters are the same as in Fig.3. The results with $a = 80$cm and $g = 3.4$ (Δ) are also shown as well as the prediction of Eq.(18) for this case ($\star$).

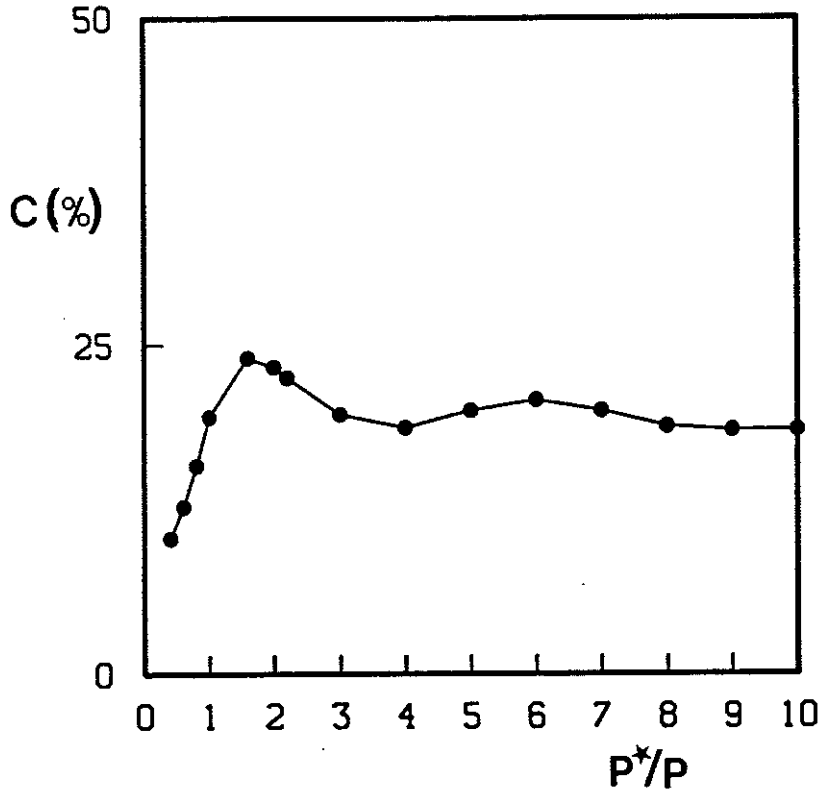

Fig.6 C as a function of P^*/P where P^* is obtained from P by multiplying it by a real number. The parameters are the same as in Fig.3 but $a = 80$cm.

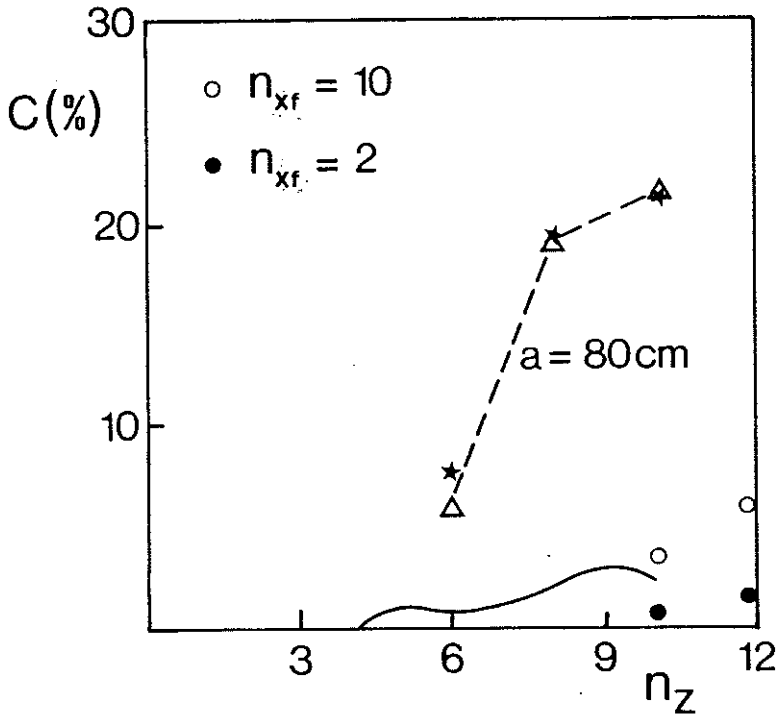

Fig.7 C as a function of n_z for the case of Fig.3 (solid line). A few results with the predetermined $n_{xf} = 10$ (o) are shown for higher n_z. The result with $a = 80$cm (Δ) is also depicted together with the prediction of the estimate of Eq.(18) ($\star$).

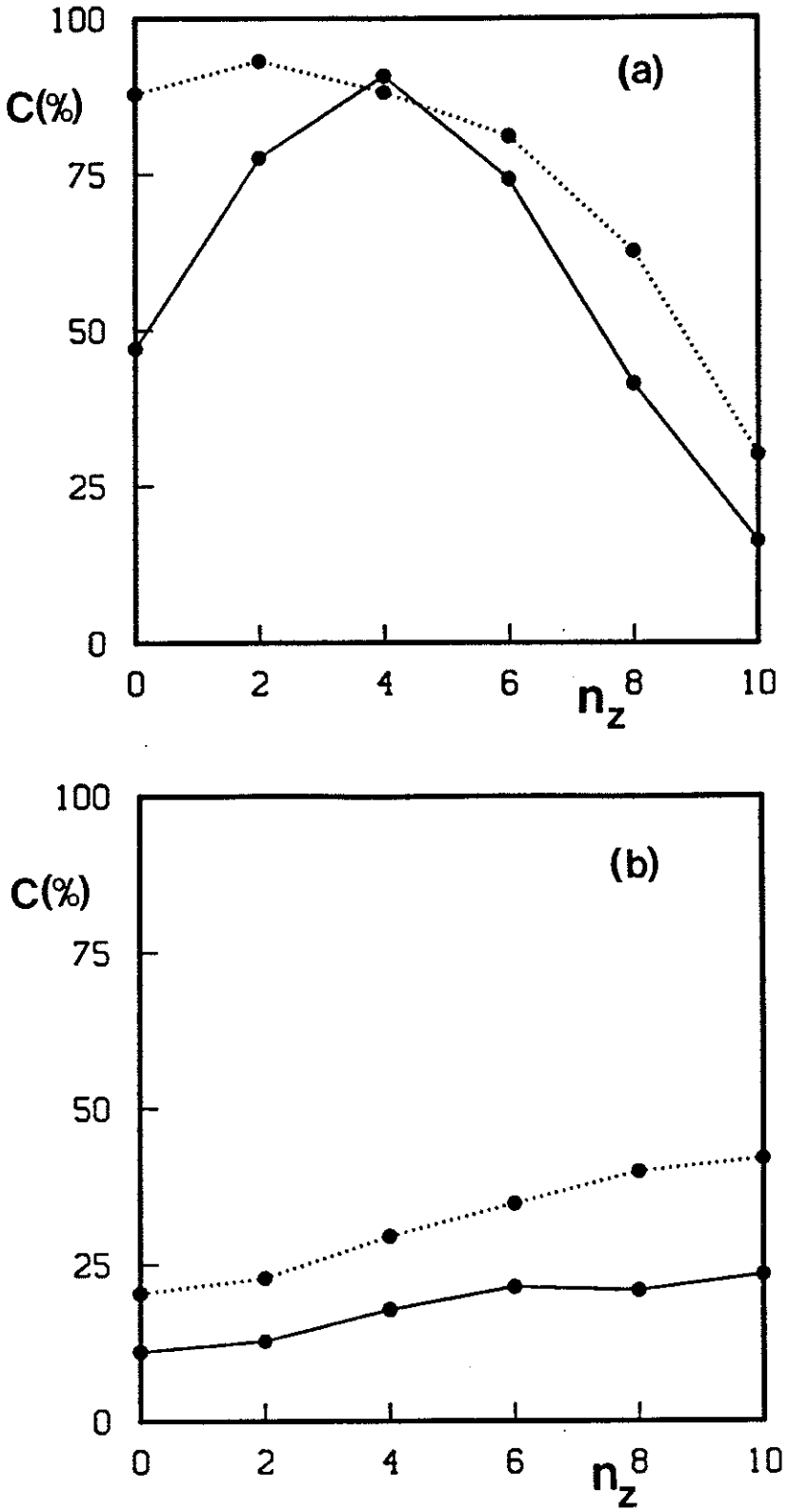

Fig.8 C as a function of n_z for D-T plasma with first harmonic heating of tritium with wall reflection (a) and without (b). An electron density profile $N(x) = 2 \times 10^{19}[1 - x(\mathrm{m})/0.2]\mathrm{m}^{-3}$ is chosen with equal amounts of deuterium and tritium extending from $x = 0$ to $x = L = 0.1\mathrm{m}$ which defines the calculation region. The wall is taken to be at $x = L+a$ with $a = 10\mathrm{cm}$. $T = 500\mathrm{eV}$ and the magnetic field dependence $5.15\mathrm{Tesla}R/(R - x(\mathrm{m}))$ with $R = 2\mathrm{m}$ are assumed and $\omega = 2.1 \times 10^8\mathrm{s}^{-1}$. The result is shown for the Airy (solid line) and the homogeneous (dotted line) boundary conditions for the fast wave.

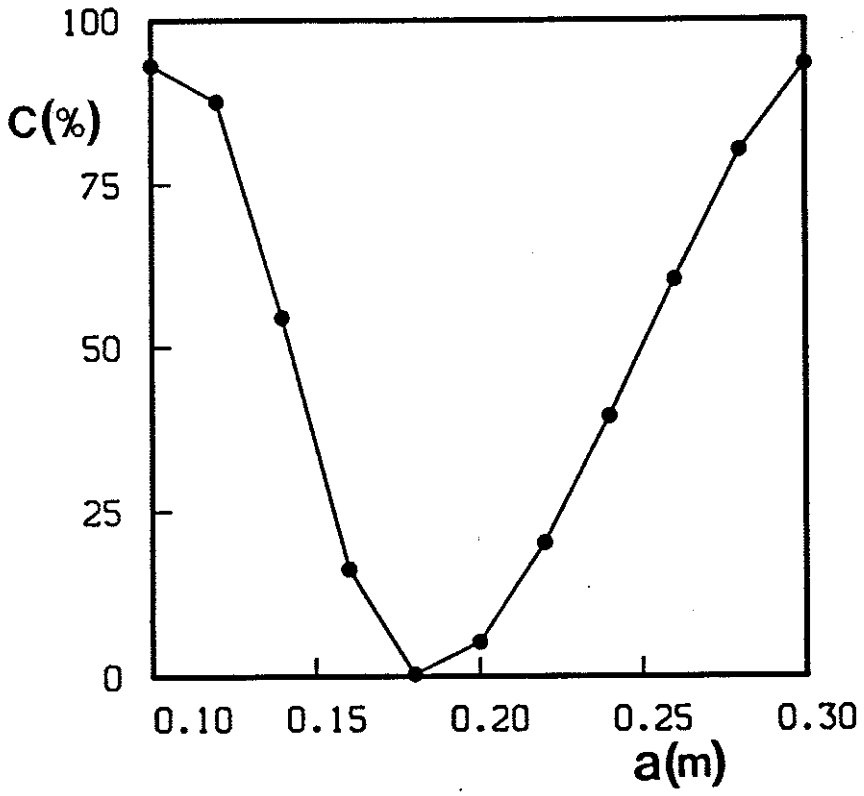

Fig.9 C as a function of a for the case of Fig.8a with the homogeneous boundary conditions.

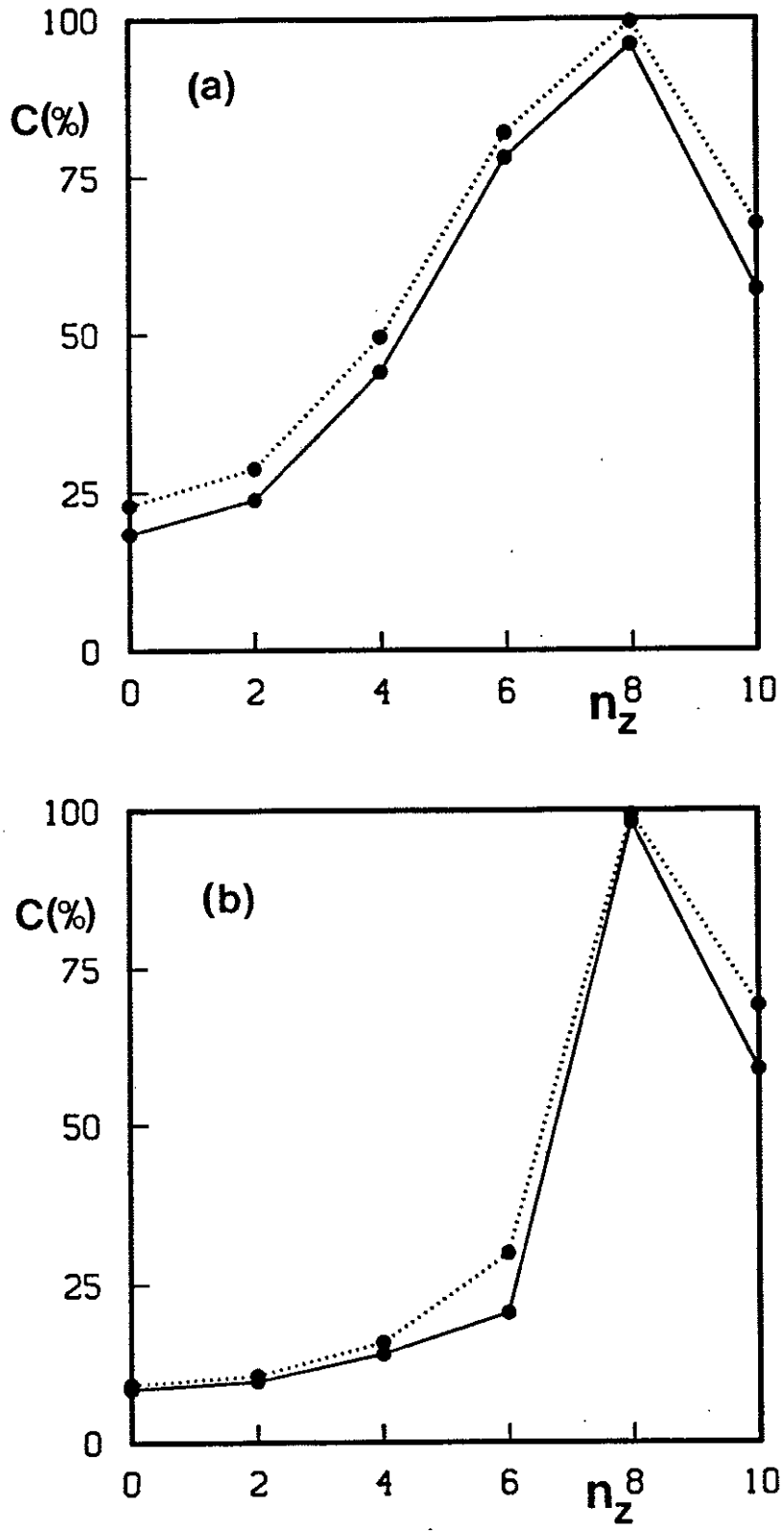

Fig.10 C as a function of n_z for ^{3}He-H plasma with first harmonic heating of ^{3}He with wall reflection (a) and without it (b). An electron density profile $N(x) = 4 \times 10^{19}[1 - x(\mathrm{m})/0.2]\mathrm{m}^{-3}$ is chosen with the abundancies 33.3% for ^{3}He and 66.7% for H. $L = 0.15$m and $a = 0.05$m are taken. $T = 500$eV and the magnetic field dependence $5.15\mathrm{Tesla}R/(R - x(\mathrm{m}))$ with $R = 2$m are assumed and $\omega = 4.2 \times 10^8\mathrm{s}^{-1}$. The result is shown for the Airy (solid line) and the homogeneous (dotted line) boundary conditions for the fast wave.

APPENDIX 1.

THE JET TEAM

JET Joint Undertaking, Abingdon, Oxon, OX14 3EA, U.K.

J.M.Adams[1], F.Alladio[4], H.Altmann, R.J.Anderson, G.Appruzzese, W.Bailey, B.Balet, D.V.Bartlett, L.R.Baylor[24], K.Behringer, A.C.Bell, P.Bertoldi, E.Bertolini, V.Bhatnagar, R.J.Bickerton, A.Boileau[3], T.Bonicelli, S.J.Booth, G.Bosia, M.Botman, D.Boyd[31], H.Brelen, H.Brinkschulte, M.Brusati, T.Budd, M.Bures, T.Businaro[4], H.Buttgereit, D.Cacaut, C.Caldwell-Nichols, D.J.Campbell, P.Card, J.Carwardine, G.Celentano, P.Chabert[27], C.D.Challis, A.Cheetham, J.Christiansen, C.Christodoulopoulos, P.Chuilon, R.Claesen, S.Clement[30], J.P.Coad, P.Colestock[6], S.Conroy[13], M.Cooke, S.Cooper, J.G.Cordey, W.Core, S.Corti, A.E.Costley, G.Cottrell, M.Cox[7], P.Cripwell[13], F.Crisanti[4], D.Cross, H.de Blank[16], J.de Haas[16], L.de Kock, E.Deksnis, G.B.Denne, G.Deschamps, G.Devillars, K.J.Dietz, J.Dobbing, S.E.Dorling, P.G.Doyle, D.F.Düchs, H.Duquenoy, A.Edwards, J.Ehrenberg[14], T.Elevant[12], W.Engelhardt, S.K.Erents[7], L.G.Eriksonn[5], M.Evrard[2], H.Falter, D.Flory, M.Forrest[7], C.Froger, K.Fullard, M.Gadeberg[11], A.Galetsas, R.Galvao[8], A.Gibson, R.D.Gill, A.Gondhalekar, C.Gordon, G.Gorini, C.Gormezano, N.A.Gottardi, C.Gowers, B.J.Green, F.S.Griph, M.Gryzinski[26], R.Haange, G.Hammett[6], W.Han[9], C.J.Hancock, P.J.Harbour, N.C.Hawkes[7], P.Haynes[7], T.Hellsten, J.L.Hemmerich, R.Hemsworth, R.F.Herzog, K.Hirsch[14], J.Hoekzema, W.A.Houlberg[24], J.How, M.Huart, A.Hubbard, T.P.Hughes[32], M.Hugon, M.Huguet, J.Jacquinot, O.N.Jarvis, T.C.Jernigan[24], E.Joffrin, E.M.Jones, L.P.D.F.Jones, T.T.C.Jones, J.Källne, A.Kaye, B.E.Keen, M.Keilhacker, G.J.Kelly, A.Khare[15], S.Knowlton, A.Konstantellos, M.Kovanen[21], P.Kupschus, P.Lallia, J.R.Last, L.Lauro-Taroni, M.Laux[33], K.Lawson[7], E.Lazzaro, M.Lennholm, X.Litaudon, P.Lomas, M.Lorentz-Gottardi[2], C.Lowry, G.Magyar, D.Maisonnier, M.Malacarne, V.Marchese, P.Massmann, L.McCarthy[28], G.McCracken[7], P.Mendonca, P.Meriguet, P.Micozzi[4], S.F.Mills, P.Millward, S.L.Milora[24], A.Moissonnier, P.L.Mondino, D.Moreau[17], P.Morgan, H.Morsi[14], G.Murphy, M.F.Nave, M.Newman, L.Nickesson, P.Nielsen, P.Noll, W.Obert, D.O'Brien, J.O'Rourke, M.G.Pacco-Düchs, M.Pain, S.Papastergiou, D.Pasini[20], M.Paume[27], N.Peacock[7], D.Pearson[13], F.Pegoraro, M.Pick, S.Pitcher[7], J.Plancoulaine, J-P.Poffé, F.Porcelli, R.Prentice, T.Raimondi, J.Ramette[17], J.M.Rax[27], C.Raymond, P-H.Rebut, J.Removille, F.Rimini, D.Robinson[7], A.Rolfe, R.T.Ross, L.Rossi, G.Rupprecht[14], R.Rushton, P.Rutter, H.C.Sack, G.Sadler, N.Salmon[13], H.Salzmann[14], A.Santagiustina, D.Schissel[25], P.H.Schild, M.Schmid, G.Schmidt[6], R.L.Shaw, A.Sibley, R.Simonini, J.Sips[16], P.Smeulders, J.Snipes, S.Sommers, L.Sonnerup, K.Sonnenberg, M.Stamp, P.Stangeby[19], D.Start, C.A.Steed, D.Stork, P.E.Stott, T.E.Stringer, D.Stubberfield, T.Sugie[18], D.Summers, H.Summers[20], J.Taboda-Duarte[22], J.Tagle[30], H.Tamnen, A.Tanga, A.Taroni, C.Tebaldi[23], A.Tesini, P.R.Thomas, E.Thompson, K.Thomsen[11], P.Trevalion, M.Tschudin, B.Tubbing, K.Uchino[29], E.Usselmann, H.van der Beken, M.von Hellermann, T.Wade, C.Walker, B.A.Wallander, M.Walravens, K.Walter, D.Ward, M.L.Watkins, J.Wesson, D.H.Wheeler, J.Wilks, U.Willen[12], D.Wilson, T.Winkel, C.Woodward, M.Wykes, I.D.Young, L.Zannelli, M.Zarnstorff[6], D.Zasche[14], J.W.Zwart.

PERMANENT ADDRESS

1. UKAEA, Harwell, Oxon. UK.
2. EUR-EB Association, LPP-ERM/KMS, B-1040 Brussels, Belgium.
3. Institute National des Récherches Scientifique, Quebec, Canada.
4. ENEA-CENTRO Di Frascati, I-00044 Frascati, Roma, Italy.
5. Chalmers University of Technology, Göteborg, Sweden.
6. Princeton Plasma Physics Laboratory, New Jersey, USA.
7. UKAEA Culham Laboratory, Abingdon, Oxon. UK.
8. Plasma Physics Laboratory, Space Research Institute, Sao José dos Campos, Brazil.
9. Institute of Mathematics, University of Oxford, UK.
10. CRPP/EPFL, 21 Avenue des Bains, CH-1007 Lausanne, Switzerland.
11. Risø National Laboratory, DK-4000 Roskilde, Denmark.
12. Swedish Energy Research Commission, S-10072 Stockholm, Sweden.
13. Imperial College of Science and Technology, University of London, UK.
14. Max Planck Institut für Plasmaphysik, D-8046 Garching bei München, FRG.
15. Institute for Plasma Research, Gandhinagar Bhat Gujat, India.
16. FOM Instituut voor Plasmafysica, 3430 Be Nieuwegein, The Netherlands.
17. Commissiariat à L'Energie Atomique, F-92260 Fontenay-aux-Roses, France.
18. JAERI, Tokai Research Establishment, Tokai-Mura, Naka-Gun, Japan.
19. Institute for Aerospace Studies, University of Toronto, Downsview, Ontario, Canada.
20. University of Strathclyde, Glasgow, G4 ONG, U.K.
21. Nuclear Engineering Laboratory, Lapeenranta University, Finland.
22. JNICT, Lisboa, Portugal.
23. Department of Mathematics, Univeristy of Bologna, Italy.
24. Oak Ridge National Laboratory, Oak Ridge, Tenn., USA.
25. G.A. Technologies, San Diego, California, USA.
26. Institute for Nuclear Studies, Swierk, Poland.
27. Commissiariat à l'Energie Atomique, Cadarache, France.
28. School of Physical Sciences, Flinders University of South Australia, South Australia SO42.
29. Kyushi University, Kasagu Fukuoka, Japan.
30. Centro de Investigaciones Energeticas Medioambientales y Techalogicas, Spain.
31. University of Maryland, College Park, Maryland, USA.
32. University of Essex, Colchester, UK.
33. Akademie de Wissenschaften, Berlin, DDR.

CR 88.49.1A